Fourth Australia - New Zealand
Conference on Geomechanics,
Perth, 14-18 May 1984

Ground Settlement and Deformation Characteristics above Undermined Areas: Experiences from the Eastern U.S. Coalfields

M. KARMIS
Associate Professor, Virginia Polytechnic Institute and State University, USA
C. HAYCOCKS
Professor, Virginia Polytechnic Institute and State University, USA
and
T. TRIPLETT
Research Associate, Virginia Polytechnic Institute and State University, USA

1 INTRODUCTION

Surface subsidence is rapidly gaining emphasis as an important environmental consequence of underground coal mining in the United States. Its impact has been witnessed in both rural and urban areas and can be associated with active as well as abandoned mining operations. The damages due to this phenomenon may include land settlement and fracturing, structural damages to surface buildings or facilities and disruption or contamination of ground water supplies.

As the need for energy increases, coal production will undoubtedly be accelerated, and since over 99 percent of all subsidence recorded in the United States arises from underground coal mining, it is evident that the incidence of subsidence will increase. With this increase in production and as underground coal mining moves into more populous areas, the prediction of surface subsidence, horizontal displacements and associated damages will surely become a requisite.

To exemplify the significance of this problem, a recent U.S. Bureau of Mines report indicated that over 32,000 km^2 have been undermined in the United States in extracting coal, metals and non-metallic ores. Over one-fourth of this area, or approximately 8100 km^2, has been disturbed by subsidence, with underground mining of bituminous coal accounting for 7700 km^2 and metal and non-metallic ores accounting for 68 km^2 of disturbed land. Thus, over 99 percent of all subsidence incidents are attributed to underground coal mining. Moreover, the Bureau of Mines estimates that an additional 10,000 km^2 will be undermined in the United States by the year 2000 (Chen et al., 1982), thus expanding the considerable areas of the country which already have been affected by subsidence.

Even though, under present technological and economic conditions, subsidence prevention is not feasible, it has been demonstrated, in many coalfields that surface subsidence can be predicted and controlled, thus minimizing the deleterious effects of ground movement. Therefore, it is imperative that reliable methods of surface movement prediction and control for the United States be established. With such techniques available, ground movements can be predicted as part of the mining plan and if environmentally, economically or legally unacceptable situations are foreseen, remedial measures can be implemented.

2 TYPES OF MINING SUBSIDENCE EXPERIENCED IN THE UNITED STATES

Underground excavations disturb the natural equilibrium of the rock mass in the vicinity of the extractions, changing the distribution of loads in the medium and causing horizontal and vertical displacements. Subsidence of the ground occurs when these displacements propagate from the mine opening, through the overlying strata, to the surface and can be manifested in two principle modes of ground settlement, sinkhole and trough subsidence (Figure 1). Sinkholes, or pit subsidence, are characterized by a sudden and sometimes violent collapse of the surface and usually occur above shallow, abandoned room and pillar mines with incompetent overburden; in some instances, however, this type of subsidence can also occur over active mines, given the proper conditions. Pit subsidence is expressed by an abrupt drop in the surface and has vertical to bell shaped walls. The washing of bedrock and surficial deposits into the mine void may cause the depth of the sinkhole to exceed the mining height.

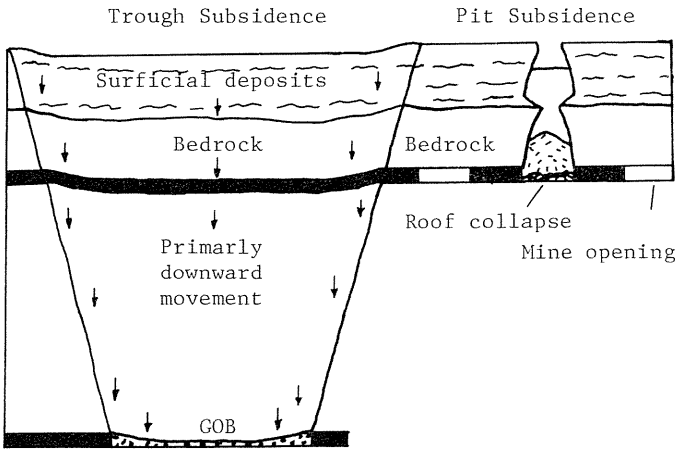

Figure 1: Trough and pit subsidence (after Wildanger et al., 1980).

Obviously, the effects of pit subsidence can be serious. However, the damage caused is the result of a loss of support over all or part of the structure. Also, due to the uncertainty of mine and geologic parameters the time, location and extent of such a subsidence event is nearly impossible to predict. Furthermore, the goal of subsidence and strain prediction is to minimize the cost of extracting coal in active mines that are below structures which may be damaged; therefore, the characteristics of trough subsidence have been more extensively studied.

Trough subsidence is expressed by a gradual and general movement over an observed area with a three-dimensional subsidence basin being formed. Trough theory considers the phenomenon of subsidence to be represented by a complicated combination of material movement and interaction, as depicted in Figure 2. Caving occurs above the mine opening, with a dome being formed above the excavation. The strata above this dome moves toward the excavation, experiencing beam bending phenomena and fracturing. However, this complicated representation of ground movement around a mining excavation is considerably complex to analyze and model; therefore, the theory is simplified by treating only the effects of underground extractions on the movement of the surface.

Trough theory considers a zone of influence in which movement occurs and which spreads from the excavation to the surface, forming a subsidence trough. When an excavation is made at depth movement of the strata extends to the surface and manifests itself as vertical displacement (subsidence) and horizontal displacement within the zone of influence. The zone of influence is bounded by a plane that extends from the edge of the extraction to the line on the surface where movement ceases. A vertical cross-section of the subsidence trough along with associated parameters is shown in Figure 3. The plane of influence is represented by line AB. The angle defined by the vertical from the rib and the line of influence is the angle of draw, γ.

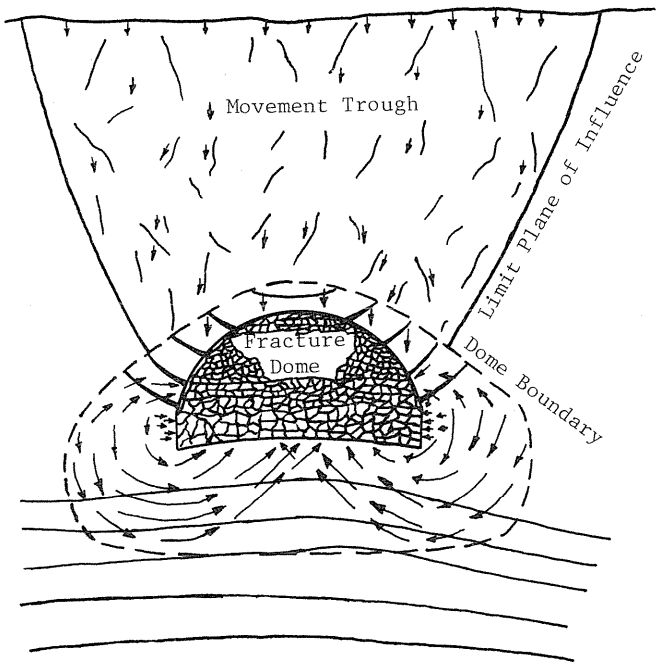

Figure 2: Strata fracture and flow caused by an underground excavation (after Denkhaus, 1964).

Within the zone of influence various patterns of ground movement exist. From B to C the vertical and horizontal movements gradually increase, with the resultant horizontal strains being tensile. At C the maximum tensile strain occurs. Point D is the inflection point, where the shape of the curve changes from convex to concave, and is the point of half-maximum subsidence. Between points C and D the subsidence increases sharply and the tensile strain decreases until it reaches zero at the inflection point. From D to E the subsidence increases further to reach a maximum at E. The strain in this region is compressive, increasing from zero at the inflection point to a maximum somewhere between D and E, then decreasing to zero at E. In the region EE the subsidence is constant; therefore, the horizontal strain is zero. The profile is symmetrical about the centerline.

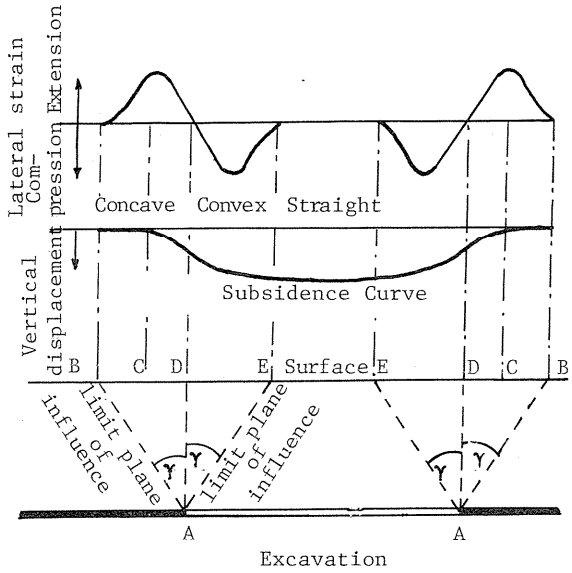

Figure 3: Trough theory concepts (after Roberts, 1981).

3 DEVELOPMENT OF AN EMPIRICAL SUBSIDENCE PREDICTION MODEL

As a requisite to any empirical study, available case studies must be identified and analyzed. During this investigation, a major effort was undertaken to develop a comprehensive data bank on mining subsidence which can be utilized to establish regional subsidence characteristics in the United States. Subsidence depends on local geologic and tectonic regimes, strata properties and mining methods, thereby exhibiting regional trends. Therefore, substantial differences in subsidence development and characteristics can be expected between foreign and domestic observations, as well as between observations from the various coalfields within the United States.

In order to develop a regionalized data bank, numerous coal companies were contacted to contribute any information that might be of value to this study. This information was supplemented by published mining subsidence data. The success of this phase of the study is indicated by the substantial number of case studies retrieved, particularly with reference to longwall panels in Appalachia.

These case studies were used to establish some basic ground movement relationships and to evaluate and validate the various methods of subsidence prediction and control in a given area. Analysis of the subsidence information has revealed some interesting subsidence characteristics for Appalachian longwall panels.

The observed angles of draw ranged from 12 to 34 degrees; however, the angle of draw appears to approach a constant value of approximately 31 degrees at width-to-depth ratios in excess of 1.2 (Figure 4). The range of the maximum subsidence

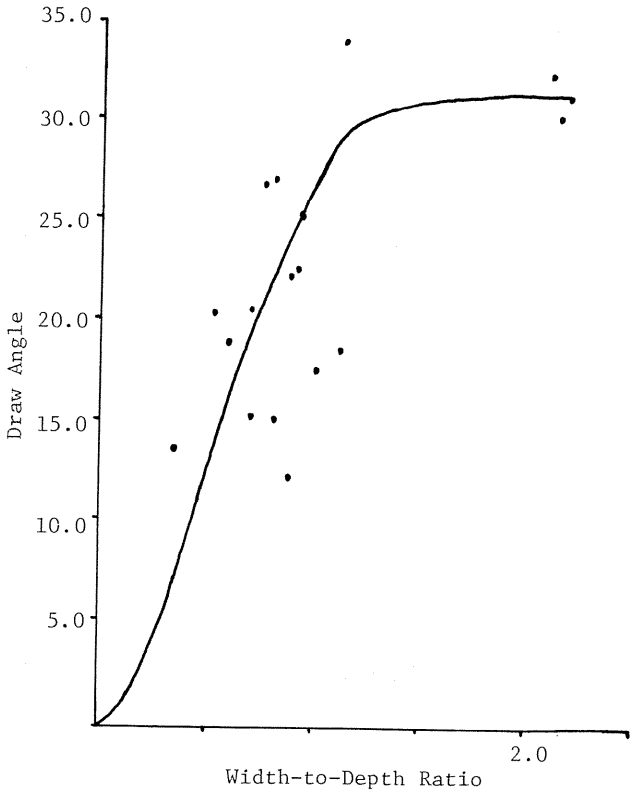

Figure 4: Variation of draw angle with Width-to-Depth ratio.

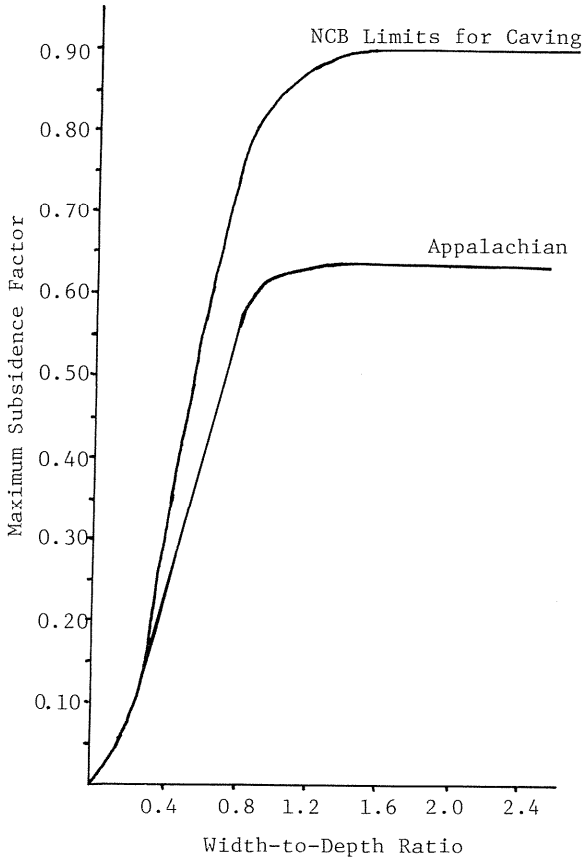

Figure 5: Influence of Width-to-Depth ratio on the maximum subsidence factor.

factors for the collected case studies is shown in Figure 5, together with the NCB limits for caving. As can be seen, this parameter also asymptotes to a constant value at a width-to-depth ratio of 1.2. These results suggest that critical conditions are reached for W/h ratios of about 1.2, as confirmed by the relationship between the position of the inflection point and the width-to-depth ratio of the panel, shown in Figure 6. It should be noted that for critical extractions the inflection point is located about 0.2 times the depth inside the ribside, whereas similar measurements in the U.K. have indicated a distance of about 0.14 times the depth. Such trends support the observation of some investigators (O'Rourke and Turner, 1981) that although smaller amounts of subsidence are experienced in the U.S., they can still induce greater curvatures and strains, in fact, as much as two to five times larger.

Once the above subsidence relationships had been established, the development of the subsidence prediction model was attempted. It was hypothesized that two factors influenced the subsidence, geology of the overburden and geometry of the panel. In order to establish the relationship between lithology and subsidence, the subsidence factor was plotted against the percent hardrock, or percent limestone and sandstone, in the overburden for critical and supercritical panels only (Figure 7). Since the effect of panel geometry had been eliminated, the relationship between subsidence and lithology could be determined. Once this correlation was known, a complete relationship between subsidence and panel geometry was possible for varying lithologies.

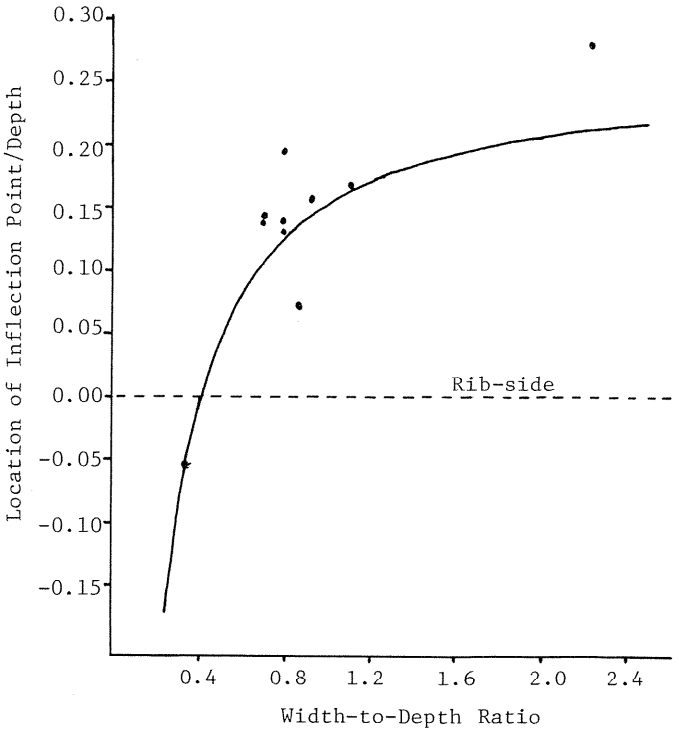

Figure 6: Effect of Width-to-Depth ratio on the position of the inflection point.

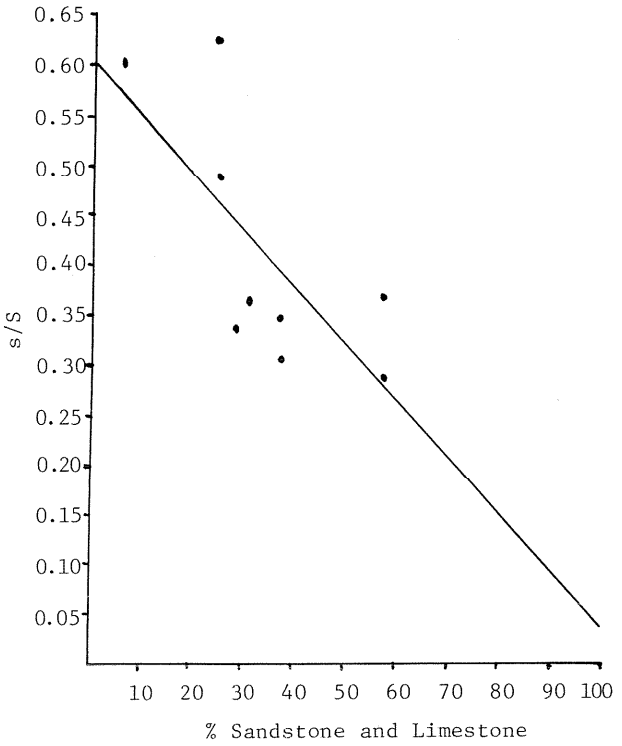

Figure 7: Influence of Sandstone and limestone on s/S for critical and supercritical panels.

Before an empirical prediction model could be developed for the Appalachian region, it was necessary to determine the characteristic subsidence profiles. To facilitate this process, all case studies were divided into either subcritical or critical (including supercritical) extractions. From these profiles a mean value curve was calculated. A hyperbolic tangent function was then chosen to mathematically describe these curves, where the subsidence, s, is given as:

$$s(x) = 0.5\ S\ [1 - \tanh\ (cx/B)] \quad . \ . \ . \ . \ . \ . \ (1)$$

where,

x = distance from the inflection point to the point in question.

B = distance from the inflection point to the centerline.

c = constant, 1.4 for subcritical panels 1.8 for critical and supercritical panels.

Using the previously described subsidence relationships, a table can be formed which presents the maximum subsidence factor as a function of the panel geometry and overburden geology (Table 1). The hyperbolic tangent function can then be used to form a second table which calculates the subsidence at any point as a function of the maximum subsidence, panel width-to-depth ratio and distance from the centerline (Table 2). Therefore, these two tables can be used in conjunction to develop the complete subsidence profile for mining conditions in the Appalachian coalfield.

4 DEVELOPMENT OF THE STRAIN PREDICTION MODEL

One of the most damaging manifestations of surface subsidence is the development of horizontal strains. As noted previously, the subsidences found in Appalachia are much smaller than those found in certain other coalfields, such as the U.K. However, the strains experienced in the U.S. are as much as two to five times greater than those predicted for British conditions. Thus, an effort was directed toward the identification of the cause of these higher strains and toward the subsequent formulation of an acceptable strain prediction model for Appalachia.

As a first step, the relationship between strain and curvature had to be determined. To accomplish this task several known relationships from various coalfields were studied and compared to strain data available from the United States. Figure 8 shows the plot of strain versus curvature for the Silesian coalfield Poland, the Chinese coalfields and the British coalfields along with the U.S. data. Two interesting notes arise from an analysis of this graph. First, there is a considerable difference between the relationships found for U.S. conditions and that derived from British data. With respect to strain, the domestic observations are closer to the values quoted for the Silesian coalfield. Second, the relationship in each case is the same, being nonlinear, where the strain is proportional to the square root of curvature.

Through a statistical analysis of the U.S. data, it was found that:

$$\text{strain} = 0.92\ (\text{curvature})^{1/2} \quad . \ . \ . \ . \ . \ . \ . \ (2).$$

Since the subsidence of any point along the profile is given as a function of x, the curvature of the profile can be found by taking the second derivative of s(x) with respect to x in the hyperbolic tangent equation, i.e.:

$$d^2s(x)/dx^2 = (c/B)^2 S\ \text{sech}^2(cx/B)\tanh(cx/B) \quad . \ . \ (3),$$

which is the equation for curvature of any point along the profile. Thus, the strain at any point is given by:

$$e(x) = 0.92\ c/B(S\ \text{sech}^2(cx/B)\tanh(cx/B))^{1/2} \quad . \ . \ (4).$$

TABLE I

MAXIMUM SUBSIDENCE AS A PERCENT OF SEAM THICKNESS									
	PERCENT HARD ROCK								
WH	10	20	30	40	50	60	70	80	90
0.00	0.000	0.000	0.000	0.000	0.000	0.000	0.000	0.000	0.000
0.05	0.005	0.005	0.004	0.004	0.003	0.003	0.002	0.002	0.002
0.10	0.020	0.018	0.016	0.015	0.013	0.012	0.010	0.008	0.007
0.15	0.043	0.040	0.036	0.033	0.029	0.025	0.022	0.018	0.015
0.20	0.075	0.069	0.063	0.056	0.050	0.044	0.038	0.031	0.025
0.25	0.113	0.104	0.095	0.085	0.076	0.066	0.057	0.047	0.038
0.30	0.156	0.143	0.130	0.117	0.104	0.091	0.078	0.065	0.052
0.35	0.203	0.186	0.169	0.152	0.135	0.118	0.102	0.085	0.068
0.40	0.251	0.230	0.209	0.188	0.167	0.146	0.126	0.105	0.084
0.45	0.298	0.273	0.249	0.224	0.199	0.174	0.149	0.125	0.100
0.50	0.344	0.316	0.287	0.258	0.230	0.201	0.173	0.144	0.115
0.55	0.388	0.356	0.323	0.291	0.259	0.227	0.194	0.162	0.130
0.60	0.428	0.392	0.357	0.321	0.285	0.250	0.214	0.179	0.143
0.65	0.464	0.425	0.387	0.348	0.309	0.271	0.232	0.194	0.155
0.70	0.495	0.454	0.413	0.372	0.330	0.289	0.248	0.207	0.166
0.75	0.522	0.479	0.435	0.392	0.348	0.305	0.262	0.218	0.175
0.80	0.545	0.499	0.454	0.409	0.364	0.318	0.273	0.228	0.182
0.85	0.563	0.517	0.470	0.423	0.376	0.329	0.282	0.236	0.189
0.90	0.579	0.530	0.482	0.434	0.386	0.338	0.290	0.242	0.194
0.95	0.591	0.541	0.492	0.443	0.394	0.345	0.296	0.247	0.198
1.00	0.600	0.550	0.500	0.450	0.400	0.351	0.301	0.251	0.201
1.10	0.612	0.561	0.511	0.460	0.409	0.358	0.307	0.256	0.205
1.20	0.619	0.568	0.516	0.465	0.413	0.362	0.310	0.259	0.207
1.30	0.623	0.571	0.519	0.467	0.416	0.364	0.312	0.260	0.208
1.40	0.624	0.572	0.520	0.469	0.417	0.365	0.313	0.261	0.209
1.50	0.625	0.573	0.521	0.469	0.417	0.365	0.313	0.261	0.209
1.60	0.625	0.573	0.521	0.469	0.417	0.365	0.313	0.261	0.209
1.70	0.625	0.573	0.521	0.469	0.417	0.365	0.313	0.261	0.209
1.80	0.625	0.573	0.521	0.469	0.417	0.365	0.313	0.261	0.209
1.90	0.625	0.573	0.521	0.469	0.417	0.365	0.313	0.261	0.209
2.00	0.625	0.573	0.521	0.469	0.417	0.365	0.313	0.261	0.209
2.20	0.625	0.573	0.521	0.469	0.417	0.365	0.313	0.261	0.209
2.40	0.625	0.573	0.521	0.469	0.417	0.365	0.313	0.261	0.209
2.60	0.625	0.573	0.521	0.469	0.417	0.365	0.313	0.261	0.209
2.80	0.625	0.573	0.521	0.469	0.417	0.365	0.313	0.261	0.209
3.00	0.625	0.573	0.521	0.469	0.417	0.365	0.313	0.261	0.209

TABLE II

DISTANCE FROM THE CENTER OF THE PANEL IN TERMS OF DEPTH													
	SUBSIDENCE AS A PERCENT OF MAXIMUM SUBSIDENCE												
W/H	0	.05	.1	.2	.3	.4	.5	.6	.7	.8	.9	.95	1.00
0.00	0.319	0.221	0.197	0.171	0.154	0.140	0.127	0.114	0.100	0.084	0.061	0.042	0.000
0.05	0.340	0.236	0.210	0.182	0.164	0.149	0.135	0.122	0.107	0.090	0.065	0.044	0.000
0.10	0.362	0.251	0.224	0.194	0.174	0.159	0.144	0.129	0.114	0.095	0.069	0.047	0.000
0.15	0.384	0.266	0.237	0.206	0.185	0.168	0.153	0.137	0.121	0.101	0.073	0.050	0.000
0.20	0.407	0.282	0.251	0.218	0.196	0.178	0.162	0.146	0.128	0.107	0.078	0.053	0.000
0.25	0.431	0.298	0.266	0.231	0.208	0.189	0.171	0.154	0.136	0.113	0.082	0.056	0.000
0.30	0.455	0.315	0.281	0.244	0.219	0.199	0.181	0.163	0.143	0.120	0.087	0.059	0.000
0.35	0.479	0.332	0.296	0.257	0.231	0.210	0.191	0.171	0.151	0.126	0.091	0.063	0.000
0.40	0.505	0.350	0.312	0.270	0.243	0.221	0.201	0.180	0.159	0.133	0.096	0.066	0.000
0.45	0.530	0.367	0.328	0.284	0.256	0.232	0.211	0.190	0.167	0.140	0.101	0.069	0.000
0.50	0.557	0.386	0.344	0.298	0.268	0.244	0.221	0.199	0.175	0.147	0.106	0.073	0.000
0.55	0.584	0.404	0.360	0.313	0.281	0.256	0.232	0.209	0.184	0.154	0.111	0.076	0.000
0.60	0.611	0.423	0.377	0.328	0.295	0.268	0.243	0.219	0.192	0.161	0.116	0.080	0.000
0.65	0.639	0.443	0.395	0.343	0.308	0.280	0.254	0.229	0.201	0.168	0.122	0.084	0.000
0.70	0.668	0.463	0.412	0.358	0.322	0.292	0.266	0.239	0.210	0.176	0.127	0.087	0.000
0.75	0.697	0.483	0.431	0.374	0.336	0.305	0.277	0.249	0.219	0.184	0.133	0.091	0.000
0.80	0.727	0.504	0.449	0.390	0.350	0.318	0.289	0.260	0.229	0.191	0.138	0.095	0.000
0.85	0.757	0.525	0.468	0.406	0.365	0.332	0.301	0.271	0.238	0.199	0.144	0.099	0.000
0.90	0.788	0.546	0.487	0.423	0.380	0.345	0.313	0.282	0.248	0.208	0.150	0.103	0.000
0.95	0.820	0.568	0.506	0.439	0.395	0.359	0.326	0.293	0.258	0.216	0.156	0.107	0.000
1.00	0.852	0.590	0.526	0.457	0.411	0.373	0.339	0.305	0.268	0.224	0.162	0.111	0.000
1.10	0.918	0.636	0.567	0.492	0.442	0.402	0.365	0.328	0.289	0.242	0.175	0.120	0.000
1.20	0.986	0.683	0.609	0.529	0.475	0.432	0.392	0.353	0.310	0.260	0.188	0.129	0.000
1.30	1.057	0.732	0.653	0.566	0.509	0.463	0.420	0.378	0.333	0.278	0.201	0.138	0.000
1.40	1.130	0.783	0.698	0.605	0.544	0.495	0.449	0.404	0.355	0.298	0.215	0.148	0.000
1.50	1.205	0.835	0.744	0.646	0.581	0.528	0.479	0.431	0.379	0.317	0.229	0.158	0.000
1.60	1.282	0.888	0.792	0.687	0.618	0.561	0.510	0.459	0.404	0.338	0.244	0.168	0.000
1.70	1.362	0.944	0.841	0.730	0.657	0.596	0.542	0.487	0.429	0.359	0.259	0.178	0.000
1.80	1.444	1.001	0.892	0.774	0.696	0.632	0.574	0.517	0.454	0.380	0.275	0.189	0.000
1.90	1.529	1.059	0.944	0.819	0.737	0.669	0.608	0.547	0.481	0.403	0.291	0.200	0.000
2.00	1.615	1.119	0.998	0.866	0.779	0.707	0.642	0.578	0.508	0.426	0.308	0.211	0.000
2.20	1.796	1.244	1.109	0.963	0.866	0.786	0.714	0.642	0.565	0.473	0.342	0.235	0.000
2.40	1.985	1.376	1.226	1.064	0.957	0.869	0.789	0.710	0.625	0.523	0.378	0.260	0.000
2.60	2.184	1.513	1.349	1.171	1.053	0.956	0.868	0.781	0.687	0.575	0.416	0.286	0.000
2.80	2.392	1.658	1.477	1.282	1.153	1.047	0.951	0.856	0.753	0.630	0.456	0.313	0.000
3.00	2.610	1.808	1.612	1.399	1.258	1.143	1.038	0.933	0.821	0.687	0.497	0.341	0.000

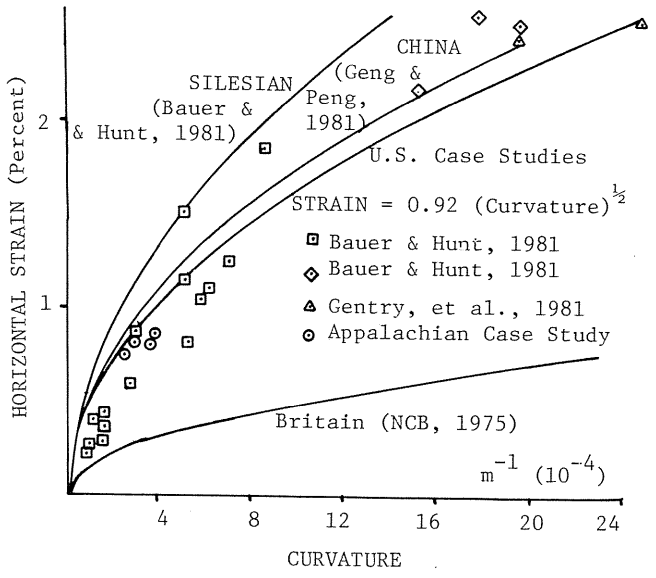

Figure 8: Relationship between horizontal strain and curvature for different coalfields.

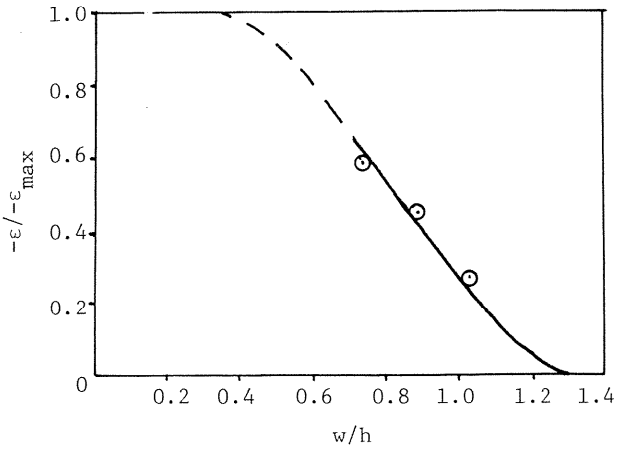

Figure 9: Effect of the Width-to-Depth ratio on the strain at the centerline of a longwall panel.

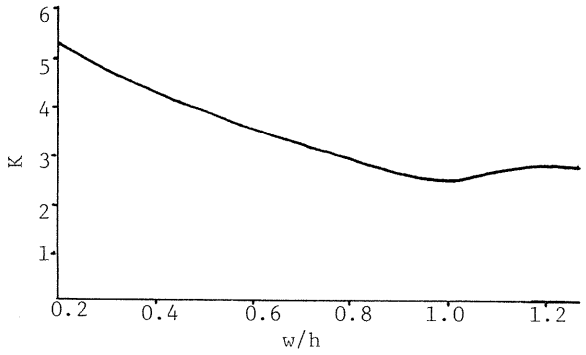

Figure 10: Effect of the Width-to-Depth ratio on K.

It should be noted that the above equation is antisymmetric about the inflection point and asymptotes to the subsidence limit and the maximum subsidence point. Case studies show that the strain is antisymmetric between the maximum strain points. Furthermore, the strain can be corrected in the tensile region using Figure 1 and in the compressive region using Figure 9. Thus, Equation 4 can be used to form Table 3, which gives the strain at any point as a function of the panel width-to-depth ratio, the maximum strain, the distance from the inflection point and the panel depth.

To use this table two values must be known, the location of the inflection point and the amount of the maximum strain. The location of the inflection point can be found from Figure 10, which gives the distance from the inflection point to the centerline as a function of the panel width and depth. The value of the maximum strain can be found from:

$$\pm e_{max} = \pm K S^{1/2}/h$$

where,

$\pm e_{max}$ = maximum tensile or compressive strain

S = subsidence at the centerline

h = depth of panel

K = constant, calculated from Figure 11.

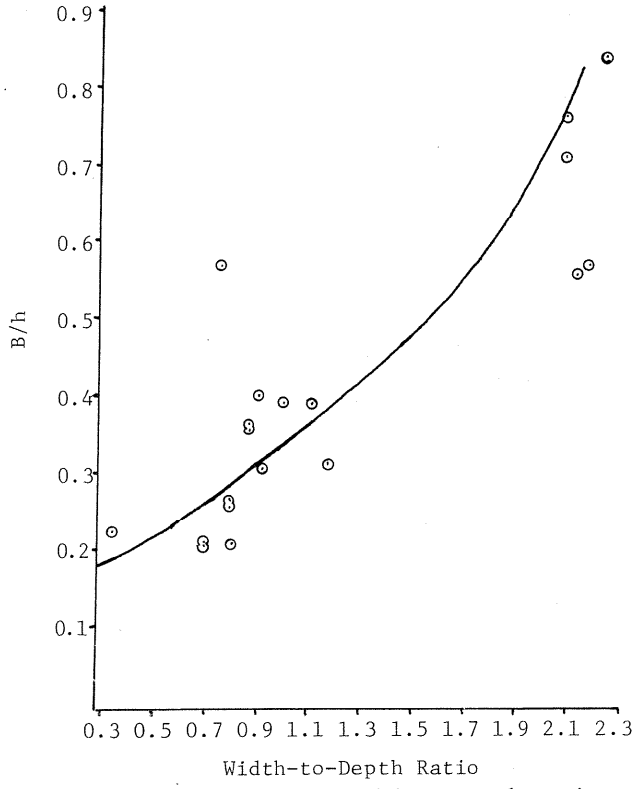

Figure 11: Effect of the Width-to-Depth ratio on B.

In order to verify the formulation of the model, the subsidence and strain for several case studies were predicted and compared to known profiles. Figure 12 shows the measured and predicted strains for the Old Ben Mine in Illinois. As can be seen, the measured strains are greater than the predicted strains in the tensile region, with the measured strains approaching the predicted strains in the compressive region. This should be expected, since the measured curvatures along the subsidence profile are greater than the predicted curvatures in the tensile region, with the measured curvatures approaching the predicted curvatures in the compressive region (Figure 13). In a situation where the measured and predicted subsidence profiles are in close agreement, as with the Appalachian case study shown in Figure 14, the strain prediction model produces an exceptional fit to the measures strain profile (Figure 15).

TABLE III

DETERMINATION OF THE STRAIN PROFILE

Extension (+ε, +x)

Values of $\varepsilon/\varepsilon_{max}$	0	0.20	0.40	0.60	0.80	1.00	0.80	0.60	0.40	0.20	0
w/h RATIO OF PANEL	DISTANCE FROM INFLECTION POINT IN TERMS OF DEPTH										
3.0	.810	.552	.424	.336	.258	.142	.058	.030	.014	.004	0
2.6	.810	.552	.424	.336	.258	.142	.058	.030	.014	.004	0
2.2	.810	.552	.424	.336	.258	.142	.058	.030	.014	.004	0
2.0	.810	.552	.424	.336	.258	.142	.058	.030	.014	.004	0
1.8	.810	.552	.424	.336	.258	.142	.058	.030	.014	.004	0
1.6	.810	.552	.424	.336	.258	.142	.058	.030	.014	.004	0
1.4	.810	.552	.424	.336	.258	.142	.058	.030	.014	.004	0
1.3	.810	.552	.424	.336	.258	.142	.058	.030	.014	.004	0
1.2	.810	.552	.424	.336	.258	.142	.058	.030	.014	.004	0
1.1	.788	.604	.482	.386	.300	.170	.070	.038	.016	.004	0
1.0	.705	.532	.425	.342	.270	.158	.066	.034	.015	.004	0
0.95	.660	.495	.395	.320	.253	.151	.063	.033	.014	.004	0
0.90	.616	.460	.368	.298	.238	.145	.060	.032	.014	.004	0
0.85	.571	.423	.339	.277	.222	.140	.058	.030	.013	.003	0
0.80	.525	.387	.311	.256	.208	.134	.056	.030	.013	.003	0
0.75	.480	.353	.285	.236	.194	.129	.053	.028	.012	.003	0
0.70	.435	.318	.259	.216	.179	.123	.050	.026	.012	.003	0
0.65	.389	.285	.233	.197	.166	.118	.049	.026	.011	.003	0
0.60	.342	.251	.208	.178	.152	.113	.047	.024	.011	.003	0
0.55	.300	.222	.186	.161	.140	.108	.045	.023	.010	.003	0
0.50	.248	.187	.161	.142	.136	.103	.042	.022	.010	.003	0
0.45	.200	.156	.138	.125	.114	.098	.041	.021	.009	.003	0
0.40	.153	.126	.116	.108	.102	.093	.038	.020	.009	.002	0
0.35	.134	.113	.105	.100	.095	.088	.037	.019	.008	.002	0
0.30	.116	.101	.095	.092	.089	.084	.034	.018	.008	.002	0
0.25	.111	.095	.090	.087	.084	.079	.033	.017	.007	.002	0
0.20	.105	.090	.085	.082	.079	.075	.032	.016	.007	.001	0

Compression (-ε, -x)

Values of $\varepsilon/\varepsilon_{max}$	0	0.20	0.40	0.60	0.80	1.00	0.80	0.60	0.40	0.20	0
w/h RATIO OF PANEL	DISTANCE FROM INFLECTION POINT IN TERMS OF DEPTH										
3.0	0	.004	.014	.030	.058	.142	.206	.254	.298	.343	.388
2.6	0	.004	.014	.030	.058	.142	.206	.254	.298	.343	.388
2.2	0	.004	.014	.030	.058	.142	.206	.254	.298	.343	.388
2.0	0	.004	.014	.030	.058	.142	.206	.254	.298	.343	.388
1.8	0	.004	.014	.030	.058	.142	.206	.254	.298	.343	.388
1.6	0	.004	.014	.030	.058	.142	.206	.254	.298	.343	.388
1.4	0	.004	.014	.030	.058	.142	.206	.254	.298	.343	.388
1.3	0	.004	.014	.030	.058	.142	.206	.254	.298	.343	.388
1.2	0	.004	.014	.030	.058	.142	.206	.254	.298	.343	.388
1.1	0	.004	.016	.038	.070	.170	.220	.262	.300	.338	
1.0	0	.004	.015	.034	.066	.158	.212	.254	.294	.332	
0.95	0	.004	.014	.033	.063	.151	.208	.252	.292		
0.90	0	.004	.014	.032	.060	.145	.206	.250	.292		
0.85	0	.003	.013	.030	.058	.140	.203	.250	.292		
0.80	0	.003	.013	.030	.056	.134	.202	.250			
0.75	0	.003	.012	.028	.053	.129	.202	.251			
0.70	0	.003	.012	.026	.050	.123	.202	.254			
0.65	0	.003	.011	.026	.049	.118	.205				
0.60	0	.003	.011	.024	.047	.113	.208				
0.55	0	.003	.010	.023	.045	.108	.216				
0.50	0	.003	.010	.022	.042	.103					
0.45	0	.003	.009	.021	.041	.098					
0.40	0	.002	.009	.020	.038	.093					
0.35	0	.002	.008	.019	.037	.088					
0.30	0	.002	.008	.018	.034	.084					
0.25	0	.002	.007	.017	.033	.079					
0.20	0	.001	.007	.016	.032	.075					

5 CONCLUSIONS

The expansion of underground coal mining into more populous areas, and the resultant increase in the potential for surface and structural damage, have rendered the formulation of accurate surface deformation models an important requisite. To meet this demand, accurate subsidence and strain prediction techniques have been formulated for the Appalachian region in the United States. The empirical subsidence prediction technique was statistically developed from a substantial number of case studies collected within the Appalachian coalfield. Using the subsidence model as a base, the strain prediction model was formulated using empirically, mathematically and mechanically derived relationships. These models can greatly facilitate mine planning and allow the amount of coal lost to the protection of surface structures to be minimized.

6 ACKNOWLEDGEMENTS

Parts of this paper are based upon work supported by the Mining and Mineral Resources Research Institutes Program, U.S. Department of the Interior. Any opinions, findings and conclusions or recommendations expressed in this publication are those of the authors and do not necessarily reflect the views of the sponsor.

The authors would like to express their appreciation to many coal companies and federal agencies for their cooperation and support in this project. Finally, acknowledgement is due to D. Hasenfus for the preparation of the manuscript.

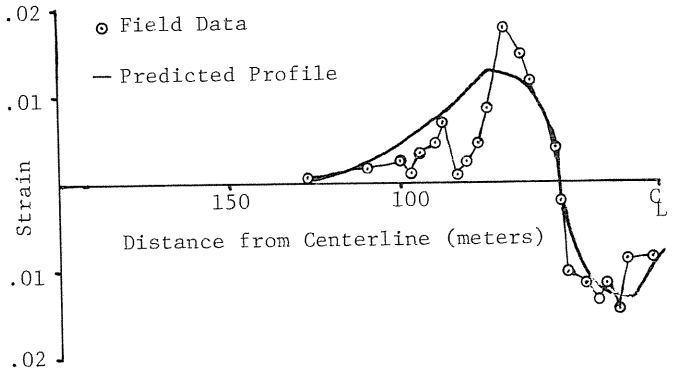

Figure 12: Predicted and measured transverse strain over the Old Ben longwall mine.

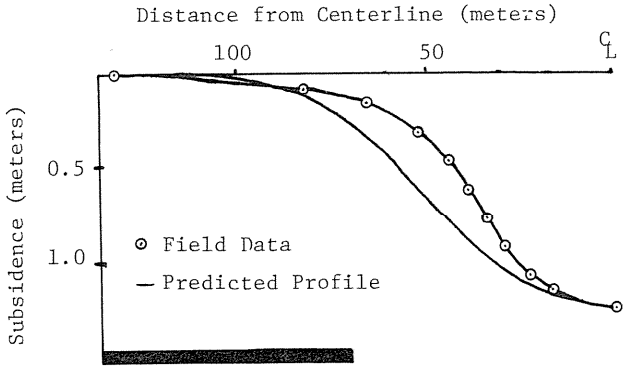

Figure 13: Predicted and measured transverse subsidence over the Old Ben longwall mine.

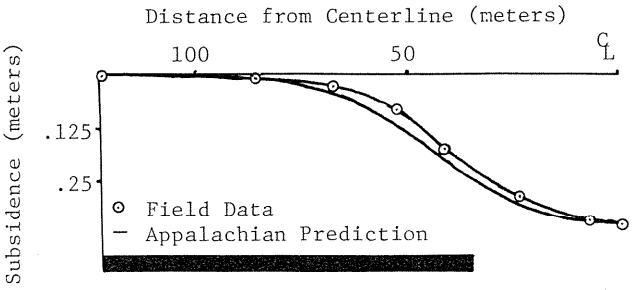

Figure 14: Predicted and measured transverse subsidence for the Appalachian longwall case study.

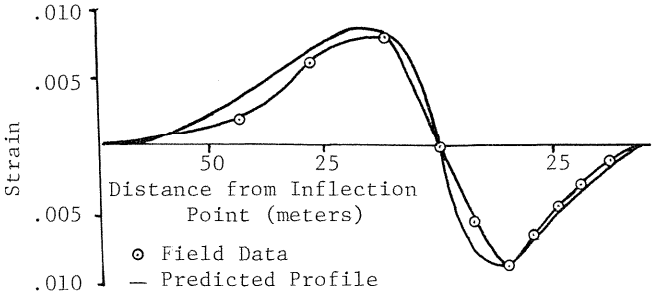

Figure 15: Predicted and measured transverse strain for the Appalachian longwall case study.

7 REFERENCES

1. BAUER, R.A. and HUNT, S.R. (1981). Profile, Strain and Time Characteristics of Subsidence from Coal Mining in Illinois. Workshop on Surface Subsidence Due to Underground Mining, Morgantown, West Virginia, pp. 207-18.

2. CHEN, C.Y., JONES, D.E. and HUNT, D.K. (1982). Government regulation of surface subsidence due to underground mining. Proceedings of an International Symposium on the State of the Art of Ground Control in Longwall Mining and Mining Subsidence, Honolulu, Hawaii, pp 245-52.

3. DENKHAUS, H.G. (1964). Critical Review of Strata Movement Theories and Their Application to Practical Problems. J. of S. African Inst. of Mining and Metallurgy, March, pp 310-32.

4. GENG, D.Y. and PENG, S.S. (1983). Longwall Mining Techniques for Minimizing Surface Structural Damage. SME-AIME Annual Meeting, Atlanta, Georgia, Preprint No. 83-99.

5. GENTRY, D.W., STEWART, C.L. and KING, R.P. (1981). Rock Mechanics Instrumentation Program for Kaiser Steel Corporation's Demonstration of Shield-Type Longwall Supports at York Canyon Mine, Raton, New Mexico, Final Report, DOE, DE-AC01-74ET12530.

6. O'ROURKE, T.D. and TURNER, S.M. (1981). Empirical methods for estimating subsidence in US coalfields. Proceedings of the 22nd International Symposium on Rock Mechanics, MIT, pp 322-7.

7. ROBERTS, A. (1981). Applied Geotechnology, Pergamon Press, Inc., New York.

8. WILDANGER, E.G., MAHAR, J. and NIETO, A. (1980). Sinkhole-type Subsidence Over Abandoned Coal Mines in St. David, Illinois, Illinois Abandoned Mined Lands Reclamation Council, 88 pp.